Heliyon 9 (2023) e18543

Contents lists available at ScienceDirect

Heliyon

journal homepage: www.cell.com/heliyon

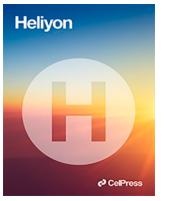

Platelet morphology, ultrastructure and function changes in acute ischemic stroke patients based on structured illumination microscopy

Bingxin Yang [a,1], Xifeng Wang [b,1], Xiaoyu Hu [c], Yao Xiao [b], Xueyu Xu [b], Xiaomei Yu [b], Min Wang [b], Honglian Luo [b], Jun Li [b,*], Yan Ma [c,**], Wei Shen [b,***]

[a] *Wuhan Puai Hospital, Tongji Medical College, Huazhong University of Science and Technology, Wuhan, Hubei, 430030, China*
[b] *Wuhan Forth Hospital, Wuhan, Hubei, 430030, China*
[c] *Wuhan Blood Center-Huazhong University of Science and Technology United Hematology Optical Imaging Center, Hubei Institute of Blood Transfusion, Wuhan Blood Center, Wuhan, Hubei, 430030, China*

ARTICLE INFO

Keywords:
Acute ischemic stroke
Structured illumination microscopy
Platelet
α-granule
Dense granule

ABSTRACT

Acute ischemic stroke (AIS) is the second leading cause of death worldwide. This study aims at assessing platelet morphology, ultrastructure and function changes of platelets in acute ischemic stroke (AIS) patients by the technique of Structured Illumination Microscopy (SIM). This assay collected platelet-rich plasma (PRP) from 11 AIS patients and 12 healthy controls. Each PRP sample was divided into 7 groups:1) rest group; 2) Thrombin-treated 5 min group; 3) Thrombin plus 2MeSAMP-treated 5 min group; 4) Thrombin plus Aspirin-treated 5 min group; 5) Thrombin-treated 1 h group; 6) Thrombin plus 2MeSAMP-treated 1 h group; 7) Thrombin plus Aspirin-treated 1 h group. SIM was applied to observe dense granules and α-granules morphology changes of platelet in AIS patients. FIJI was used to quantify the image data. We finally observed 1448 images of platelets within the 7 groups. In rest group, 7162 platelets were calculated platelet diameter, CD63 dots, average CD63-positive dots area, CD63-positive area per platelet, CD63-positive area Fov, VWF dots, average VWF-positive dots area, VWF-positive area per platelet and VWF-positive area Fov. ELISA was used to detect release of platelet factor 4 (PF4) of α-granules. The results showed that AIS patients had lower number and smaller area of platelet granules. Platelet α-granules of AIS patients concentrated to parenchymal-like fluorescent blocks in Thrombin-treated 1 h group. Antiplatelet drug treatment could reverse the concentration of platelets α-granules, and 2MeSAMP was more powerful than Aspirin in vitro. This study complemented detail information of platelet ultrastructure of AIS patients, provided a new perspective on the pathogenesis of AIS and the mechanism of antiplatelet drugs based on SIM and provided a reference for future related studies. SIM-based analysis of platelet ultrastructure may be useful for detecting antiplatelet drugs and AIS in the future.

* Corresponding author.
** Corresponding author.
*** Corresponding author.
E-mail addresses: yangbingxin@hust.edu.cn (B. Yang), whsdsyy1985313@163.com (J. Li), musketeers85@hotmail.com (Y. Ma), shenwei1971@126.com (W. Shen).
[1] Contributed equally.

https://doi.org/10.1016/j.heliyon.2023.e18543
Received 10 March 2023; Received in revised form 18 July 2023; Accepted 20 July 2023
Available online 25 July 2023

1. Introduction

In addition to being the second major cause of death in the world, acute ischemic stroke (AIS) is the most deadly sudden disease following an arterial heart attack. It is also the leading cause of disability worldwide [1,2]. AIS is primarily caused by intracranial atherosclerosis [3]. Rupture or erosion of atherosclerosis plaque generates atherothrombosis, leading to AIS eventually [4]. Platelets play a key role in this process by releasing prothrombotic factors, secreting proinflammatory factors and amplifying coagulation cascade [5]. These platelet factors are mainly stored in dense granules and α-granules of platelets and released upon platelet activation. Elevated circulation von Willebrand factor (VWF) that from endothelia cells (EC) or platelet α-granules acts as a bridge between subendothelial and platelet in AIS patients. Once adhesion to endothelium, either platelet dense granules or α-granules rapidly release numerous small molecules and proteins which amplify platelet activation, adhesion and aggregation [6,7]. Meanwhile, platelets recruit monocyte, enhance monocyte differentiation and reduce neutrophils apoptosis by releasing numerous chemokines from α-granules [8–10]. Releasing factors of platelet granules interconnect a crosstalk between thrombosis and inflammation contributing to occurrence and progression of AIS [11]. There is no doubt that the plasma level of platelet granule content increased in AIS patients [12]. However, limited resolution by light diffraction, it's still thirsty on structural changes of platelet granules of AIS patients, lacking effective assessing of changes of granule ultrastructure in AIS patients.

Platelet, the diameter only 2–5 μm, contains so many organelles such as tubulin, mitochondria, lysosome, dense granule and α-granule [13]. Dense granule and α-granule are dominant releasing organelles in AIS as mentioned above. The smallest dense granules which only 150 nm release a range of small molecules, including ADP, ATP, calcium and 5-HT, to activate more resting platelets and amplify activation effect. As the largest granule of platelet, α-granule is 200∼400 nm size containing large number of proteins such as VWF, fibrinogen, and coagulation factors V, which accelerate platelet spreading, aggregation and coagulation [13,14]. Moreover, α-granules release chemokines such as platelet factor 4 (PF4, CXCL4), CXCL5 and platelet-derived growth factor (PDGF) to promote response of thrombo-inflammation [11]. Despite their important role in AIS, it's still difficult to observe these small size structures by conventional fluorescence microscopy whose resolution is about 200∼300 nm in the lateral direction and 500–750 nm in the axial direction, which is too large to observe platelet granules in detail [15]. Some studies showed that the numbers of α-granules decreased in AIS patients by transmission electronic microscopy (TEM) [16]. Although electronic microscopy owning enough resolution, it doesn't allow for the study of single platelet and requires experienced operators. Confocal has improved the resolution of z-axis to 500 nm in recent years. Researchers has successfully observed 15 different proteins in α-granule through confocal [17]. However, confocal still can't effectively distinguish neighboring proteins when the protein density is high [18]. The small size of platelet granule and limited resolution of microscopy impose restrictions on study of platelet ultrastructure in AIS patients.

Super resolution microscopy technique has been rapidly developed in recent decades. It overcomes the limitation of diffraction through some different approaches to visualize biological samples at nanoscale [15], making it possible to evaluate granules of platelet in AIS patients. There are several kinds of super resolution microscopy with different theory, including stimulated emission depletion (STED), photoactivated localization microscopy (PALM), stochastic optical reconstruction microscopy (STORM), super-resolution fluorescence microscopy (SRM) and structured illumination microscopy (SIM) [19–22]. SIM moves unresolvable high frequency information into observable region through illuminating a sample with structured light, through which SIM achieves a resolution of ∼100 nm in the lateral direction and ∼300 nm in axial direction [23]. Subsequently, reconstructing super-resolution images by computation obtain the precise image information [24]. SIM enables efficient collection and detection of photons to ensure using minimal power to obtain images with reduced fluorescence quenching [25]. And SIM samples are easy to make - the antibodies and probes suitable for standard fluorescence microscopy can also be used for SIM [26]. Although the improved resolution is lower than some other super resolution microscopy, the doubled resolution is enough to observe platelet granules. Adding the characteristics of faster speed of imaging, SIM is capable and suitable to observe platelet granules in AIS patients. Actually, attempts have been made to use SIM to examine platelet ultrastructure in illnesses, leading to new methods for diagnosing diseases [27–29]. Therefore, SIM can also be attempted to assess platelet ultrastructure in AIS patients.

The antiplatelet drugs 2MeSAMP and Aspirin inhibit the P2Y12 receptor and cyclooxygenase-1(COX-1) synthesis, respectively. In AIS patients, platelet granules including dense granules and α-granules are essential for activating platelets while antiplatelet drugs may also affect the structure of these granules. Therefore, we used SIM to observe and analyze the two platelet granules in 7 different states of AIS patients, including 1) rest group; 2) Thrombin-treated 5 min group; 3) Thrombin plus 2MeSAMP-treated 5 min group; 4) Thrombin plus Aspirin-treated 5 min group; 5) Thrombin-treated 1 h group; 6) Thrombin plus 2MeSAMP-treated 1 h group; 7) Thrombin plus Aspirin-treated 1 h group. SIM will provide an added layer of information about platelet structure changes by observing and analyzing the ultrastructure of platelets. It may offer more details in mechanism of AIS and antiplatelet drugs. A change in the ultrastructure of platelets in elderly people might be a way of monitoring the onset of this disease. In the meantime, evaluation of platelet reactivity to various antiplatelet drugs might provide a basis for clinically individualized therapy.

2. Methods

2.1. Patients and healthy donors

Peripheral blood was obtained from consenting healthy people and AIS patients. The age of patients enrolled were over 55 years old, at the same time healthy people included the group ranging from 18 to 30 years old (young healthy = YH) and those elder than 55 years old (elderly healthy = EH) for the reason that the platelet structure and function may change with age. Other basic information of

the enrolled samples could be found in Table 1. AIS patients were included at the Department of Neurology in the Wuhan Forth Hospital, diagnosed based on Chinese stroke diagnosis and treatment guidelines (2018). We excluded patients with: (1) cerebral pathology situations including hemorrhage, vascular malformation, tumor and encephalopyosis that were found through imaging examination (CT or MRI); (2) taking any type of antiplatelet medication or drug affecting platelets in 14 days; (3) disease affecting platelets such as blood system disease, atrial fibrillation, severe liver or renal dysfunction, tumor, and immune diseases; (4) bleeding in gastrointestinal tract or major surgery within 3 months; (5) using intravenous anticoagulation or thrombolysis in the past week; (6) 2 weeks of fever or infectious disease. Informed consent forms were signed by all volunteers. The research was conducted according to relevant guidelines and regulations. It was approved by Wuhan Forth Hospital under the approval number KY2021-086-01.

2.2. Platelet preparation

The fresh obtained blood was separated within 6 h. The experimental manipulation was at room temperature unless otherwise specified. Whole blood was centrifuged for 12 min at 200×*g* with an increase and reduced speed of 1 to generated platelet-rich plasma (PRP). PRP was fixed for 30 min with Paraformaldehyde 8% Aqueous solution (8% PFA, Electron Microscopy Science, Hatfield, England, cat: 157–8) at room temperature. PRP was subsequently washed by centrifugation using Phosphate Buffered Saline (PBS, TBD science, Tianjin, China) and centrifuged at 1500×*g*, 3 min for a total of three times. For activation experiments, PRP was incubated with ACDT (10% acid-citrate dextrose and 90% Tyrode buffer, Tyrode buffer was 138 mM NaCl, 2.9 mM KCL, 2 mM $MgCl_2$, 4 mM NaH_2PO_4, 12 mM $NaHCO_3$, 5.5 mM Glucose, 10 mM HEPES, PH 7.2), or ACDT plus 10 μM 2-methyl-thioadenosine-monophosphate (2MeSAMP, Sigma-Aldrich, St. Louis, MO, USA, cat: 22,140-20-1), or ACDT plus 53 μM Aspirin (Sigma-Aldrich, St. Louis, MO, USA, cat: #MKCM5838) for 10 min at 37 °C. Then activated with 0.5U thrombin (TH, Sigma-Aldrich, St. Louis, MO, USA, cat: 9002-04-4) for either 5 min or 1 h, without stirring or agitation. The activated sample were fixed using fix buffer (8% PFA and PBS 1:1 preparation) for 15 min and then washed twice in PBS in the end.

2.3. Immunofluorescent staining

All incubation were done at room temperature unless otherwise stated. Platelets were incubated with Blocking Buffer (10% Normal Goat Serum, 0.05% Triton-X100, 89.95% PBS, 165 mM BSA) for 1 h after permeabilizing in 0.02% Triton-X100 (Sigma-Aldrich, St. Louis, MO, USA, cat: 9036-19-5). After incubation overnight with the primary antibody (Anti-CD63, abcam, Cambridge, England; lot: ab8219; Von Willebrand Factor, Dako Denmark, Glostrup, Hovedstaden, Denmark, lot: 20,067,358) at 4 °C and washed five times with

Table 1
Characteristics of AIS patients and healthy control. Patient (P), Elderly healthy people (EH), Young healthy people (YH), National Institute of Health stroke scale (NIHSS), magnetic resonance imaging (MRI), Platelet distribution width (PDW), mean platelet volume (MPV), platelet large cell ratio (*P*-LCR). The EH group were the same-age controls for the patient group. There was no significant difference in the basic information between the two sample groups. *: There was difference between AIS patients and young healthy control (YH), but no difference with EH. For age: ****P < 0.0001, for PDW: P = 0.0031; for MPV: ***P = 0.0001; for *P*-LCR: *P = 0.0116.

Number	Sex	Age	NIHSS score	MRI	Platelet number (125–350 × 109)	PDW* (15.5–18.1 fL)	MPV* (9.4–12.5 fL)	*P*-LCR* (17.5–24.3%)
P1	M	58	0	Lacunar infarction	243	16.7	12.3	10.4
P2	F	71	4	Right basal ganglia infarction	234	14.1	11.2	35
P3	M	59	3	Coronal region infarction	232	12.9	11.1	33.8
P4	M	54	6	Right cerebellar infarction	158	16.1	12.2	43.4
P5	F	85	3	Left basal ganglia infarction	217	16.5	9.4	21.9
P6	M	62	2	Right parietal lobe infarction	290	10.5	9.9	23.9
P7	M	65	4	Left parietal lobe infarction	148	15.6	11.6	38.3
P8	M	62	1	Left cerebellar hemisphere infarction	177	14.2	11.2	34.3
P9	F	83	0	Bilateral frontal infarction	258	10.8	10.0	24.4
P10	M	72	2	Left occipital lobe infarction	319	13.2	11.5	36.7
P11	M	66	6	Right radiocapillary infarction	218	10.9	10.2	25.9
EH1	M	74	/	/	223	12.4	10.5	29.3
EH2	F	62	/	/	203	13.2	11.7	37.8
EH3	M	70	/	/	288	10.9	9.9	24
EH4	M	67	/	/	206	13	10.7	30
EH5	F	65	/	/	163	17	13	48.3
EH6	M	73	/	/	201	11	9.9	23.8
YH1	F	24	/	/	253	11.1	8.9	18.5
YH2	M	25	/	/	160	10	8.9	17.8
YH3	M	22	/	/	224	10.7	9	18.9
YH4	M	26	/	/	240	10.6	9.1	18.7
YH5	F	21	/	/	209	8.5	7.9	19
YH6	M	29	/	/	293	10.6	9.1	18.7

washing buffer (1% Normal Goat Serum, 0.05% Triton-X100 and PBS), the secondary antibody (Goat Anti-Mouse IgG H&L (Alexa Fluor-488), abcam, Cambridge, England, lot: ab150113; Goat Anti-Rabbit IgG H&L (Alexa Fluor 647), abcam, Cambridge, England, lot: ab150079) was incubated in the dark for 1 h and washed again as before. The concentration of primary antibody used were 1:200 (Anti-CD63) and 1:1000 (Von Willebrand Factor). The concentration of secondary antibody were 1:500. For imaging after staining, it can also be fixed again using PFA and stored in 4 °C within 1 month for imaging.

2.4. Structured illumination

Platelet cells were acquired on the Multi-SIM imaging system (NanoInsights). This machine needs a 100×/1.49 NA oil objective (Nikon CFI SR HP Apo), solid-state single mode lasers (488 nm, 640 nm) and a COMS (Complementary Metal-Oxide-Semiconductor) camera (ORCA-Fusion C14440–20UP, HAMAMATSU). To obtain optimal images, immersion oils with refractive indices of 1.518 were used for platelet cells in glass dishes [30].

2.5. Image analysis

Images were successively taken under 488 nm (CD63) and 647 nm (VWF). A total of nine different sinusoidal illumination patterns were used to acquire SIM raw images, which were reconstructed into one image which was used to analyze finally. The microscope is routinely calibrated with 100 nm fluorescent spheres to calculate both the lateral and axial limits of image resolution. SIM image stacks were reconstructed using SI-Recon 2.11.19 (NanoInsights) with the following settings: pixel size 30.6 nm; channel-specific optical transfer functions; Wiener filter constant 0.01; discard Negative Intensities background.

Reconstructed SIM images could analyze the average diameter of platelets by FIJI. For CD63 and VWF dots, average CD63-positive and VWF-positive dots area, CD63-positive and VWF-positive area per platelet, CD63-positive and VWF positive area Fov, acquired their mean in each image and then compared. Each reconstructed picture was set with a 3 μm scale, a pixel length of 0.0306 μm, and the diameter of all platelets to be measured was labeled using Straight and ROI. Finally, Click Measure to automatically measure the diameter of platelets and exclude the incomplete platelets around the picture. For granule analysis, granules in each image were automatically segmented using the FIJI macro-encoding. Single platelet was circled from the open field image corresponding to each fluorescent image. After the fluorescence map was converted to the gray scale map, threshold was processed, the appropriate threshold size was adjusted to best distinguish the positively stained granules and the background. Using Fill Holes filled granules, watershed segmented each granule, Analyze Particles eliminated the area less than 0.01 μm^2 because they were considered background. Storage of the platelets where the measured granules were located and obtained the number and area of positive granules, the area of positive granules in each platelet and the percentage of positive granules in each field.

2.6. Detection of platelet factor 4 (PF4)

PF4 released at the platelet resting state and after activation was measured by ELISA. The supernatant of PRP after the above treatment was collected and terminated on ice for 5 min. It was subsequently centrifuged at 1000×*g* for 15 min at 4 °C, and the centrifuged supernatant was collected and stored at −80 °C for detection. Rising speed and lower speed are all 1. Assays were performed in accordance with instructions of Human PF4 ELISA kit (Cusabio, Wuhan, China, lot: CSB-E07882). The PF4 release measured after activation excepted the rest state release equals the multiple of change in PF4 release. The PF4 release measured by activation after inhibitor treatment excepted activated without any treatment for the fold change of PF4 release after inhibitor use. The final obtained data were subjected to T-test.

2.7. Statistical analysis

Prism 8.3.0 was used to analyze all the data. Data processing is anonymous. Remove incomplete, pseudopodia generated and platelets less than 2 μm in diameter. Diameters of 7162 platelets were finally analyzed (YH = 2529, EH = 2128, P = 2505). The obtained images were automatically analyzed by FIJI for analyzing platelet positive granules, include 286 CD63 images and 299 VWF images. The total area of positive granules except the number of cells is equal to the total area of positive granules per platelet. The total area of positive granules except 981.5689 μm^2 (the area of one field was 31.33 μm* 31.33 μm) to obtain the percentage of area of positive granules in one field (%area Fov). A two-tailed, unpaired student T-test was used to compare patients with healthy control subjects when data fit normal distribution. We used two-tailed Mann Whitney test or Kolmogorov-Smirnov test when the data didn't fit a normal distribution. P value < 0.05 of T-test was regarded as significant differences.

3. Results

3.1. Observation of platelet morphology and granule structure in AIS patients based on structured illumination microscopy

In this study, we observed the morphology of platelets and the structure of platelet granules by Structured Illumination Microscopy (SIM), analyzed these structures through FIJI. After conventional immunofluorescence staining, it could quickly capture high -resolution images. A total of nine images were taken under diffracted light at different angles and finally reconstructed to one picture, which would only take 5 m s. After dense granules and α-granules been stained, AIS patients' platelets and healthy control group's

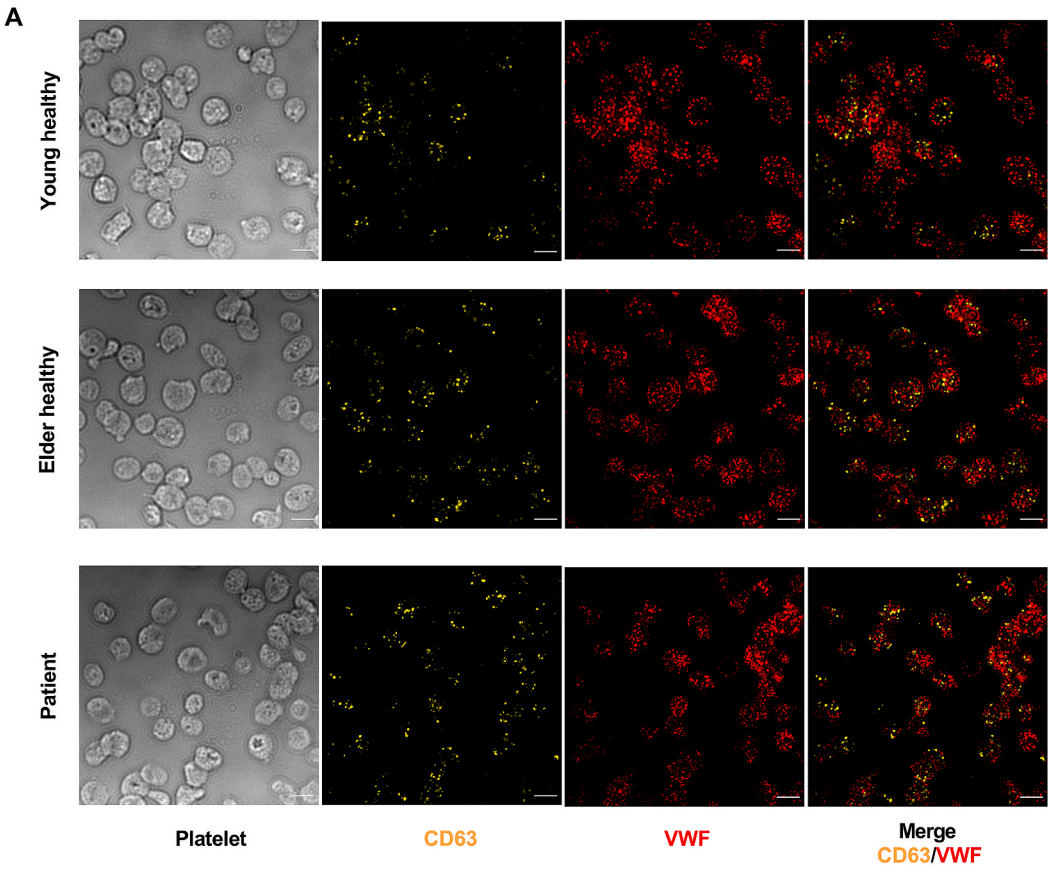

(caption on next page)

Fig. 1. Morphology and ultrastructure of resting platelets in AIS patients and healthy controls. A representative image of resting platelet is shown from young healthy (YH, n = 77), elder healthy (EH, n = 97) and AIS patient (n = 125). **A**, The images showed platelets were disc-shaped with smooth and neat edges in column 1; the dense granule and α-granule labeled with anti-CD63 (yellow) and *anti*-VWF (red) in column 2 and column 3; merge image of CD63 and VWF in column 4. The two-color images were acquired with laser light at 488 (CD63) and 642 (VWF). The data in this figure displayed oval shaped platelets with dense granule and α-granule scattered throughout. **B**, CD63 and VWF were precisely localized in platelets. CD63 threshold: a suitable threshold showed all the labeled CD63 proteins and facilitated quantitatively analysis. Scale bars: 3 μm. (For interpretation of the references to color in this figure legend, the reader is referred to the Web version of this article.)

platelets were observed and analyzed for morphology and ultrastructure based on SIM (Fig. 1A). For the purpose of avoiding bias resulted from aging, the healthy control included >55 years old healthy group (elderly healthy group, EH) and 18–30 years old healthy group (young healthy group, YH). Baseline information consisted of sex, age, National Institute of Health stroke scale (NHISS) score, MRI, platelet measurements including number, width, volume, and ratio of large platelets between patients and controls are listed in Table 1 (Table 1). Based on SIM observations, healthy controls' rest platelets were disc-shaped whose edges are smooth and neat, as do AIS patients' rest platelets (Fig. 1A). Healthy controls and AIS patients showed no obvious visual morphological changes. Moreover, it can be clearly seen that CD63 and VWF are distributed punctually in each platelet without aggregates in healthy controls (Fig. 1A). A few of VWF was in a long tubular form. At the same time, we displayed the merge image of CD63 and VWF (Fig. 1A). It's clear that the density of CD63 dots was lower than that of VWF in each platelet. Subsequently, as compared with healthy controls, there was no apparent difference in platelet ultrastructure morphology between AIS patients. The distribution of granules could be seen in the images of platelets with CD63 and VWF merge. Single platelet was distinguished by the means of merging the bright field and corresponding fluorescent field using FIJI to observe and analyze platelet granules (Fig. 1B). And appropriate threshold was selected to measure the number and area of positive granules for all stained CD63 and VWF (Fig. 1B).

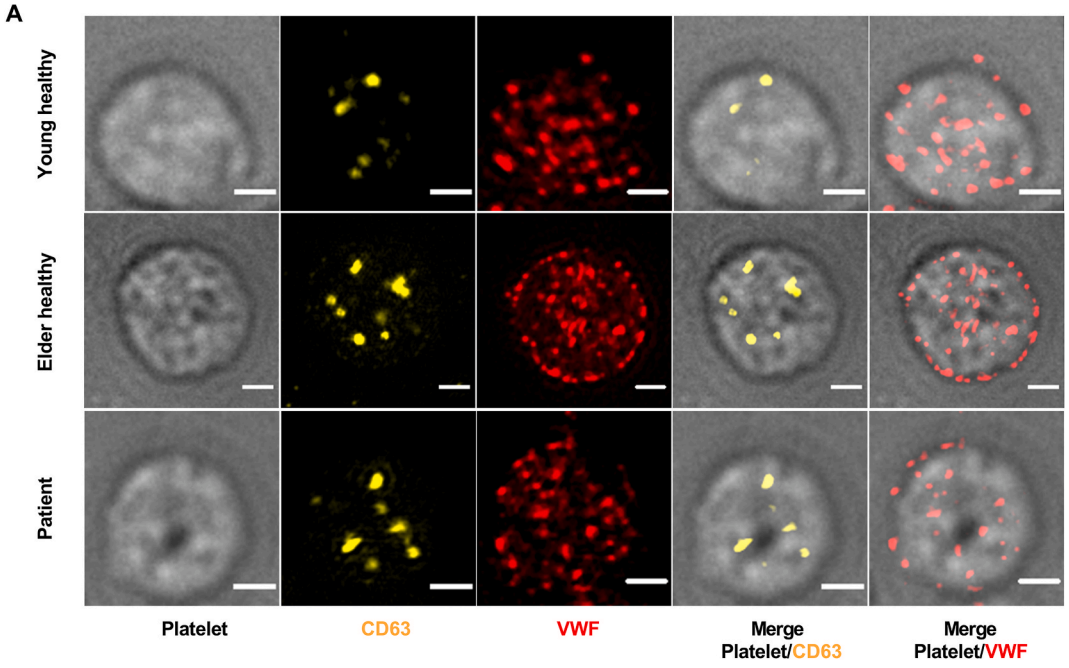

Fig. 2. Alteration in CD63 and VWF number and area in AIS patients. Quantification of dense granule (CD63) and α-granule (VWF) content of AIS patients and healthy controls. **A**, SIM image better distinguished stained CD63 (yellow) and VWF (red) in individual platelet. **B**, Platelet diameter decreased correlated with age. Comparison platelets diameter from YH (n = 2529, 6 YH), EH (n = 2128, 6 EH) and AIS patient (n = 2505, 11 P) showed platelets in elder healthy and AIS patient are smaller. ****P < 0.0001. **C**, $CD63^{+}$ objects were increased in AIS patients ((n = 78,6 YH; n = 90, 6 EH; n = 118, 11 P). *P = 0.0213, ****P < 0.0001. **D**, CD63 average size in AIS patients was lower than YH and EH, ****P < 0.0001. **E**, Quantification of CD63 area per platelet in YH, EH and AIS patient. **P = 0.004, ****P < 0.0001. **F**, Analysis of CD63 %area field of view (Fov) in YH, EH and AIS patient. **P = 0.0074, ****P < 0.0001. **J**, VWF + objects of AIS patients (n = 125,11 P) were lower than YH (n = 77, 6 YH) and EH (n = 97, 6 EH). *P=0.0418, ****P < 0.0001. **H**, VWF size of AIS patients was lower than EH. *P = 0.0107, ****P < 0.0001. **I**, VWF area per platelet in AIS patient was lower than EH. ****P < 0.0001. **J**, VWF %area field of view (Fov) decreased with age and lowest in AIS patients. YH: young healthy; EH: elder healthy; P: AIS patient. **P = 0.004, ****P < 0.0001. Data are presented as mean ± standard deviation. VWF + objects and VWF size used unpaired two-tailed T-test; $CD63^{+}$ objects used two-tailed Kolmogorov-Smirnov test; the other tests used two-tailed Mann-Whiyney test. Scale bar:1 μm. (For interpretation of the references to color in this figure legend, the reader is referred to the Web version of this article.)

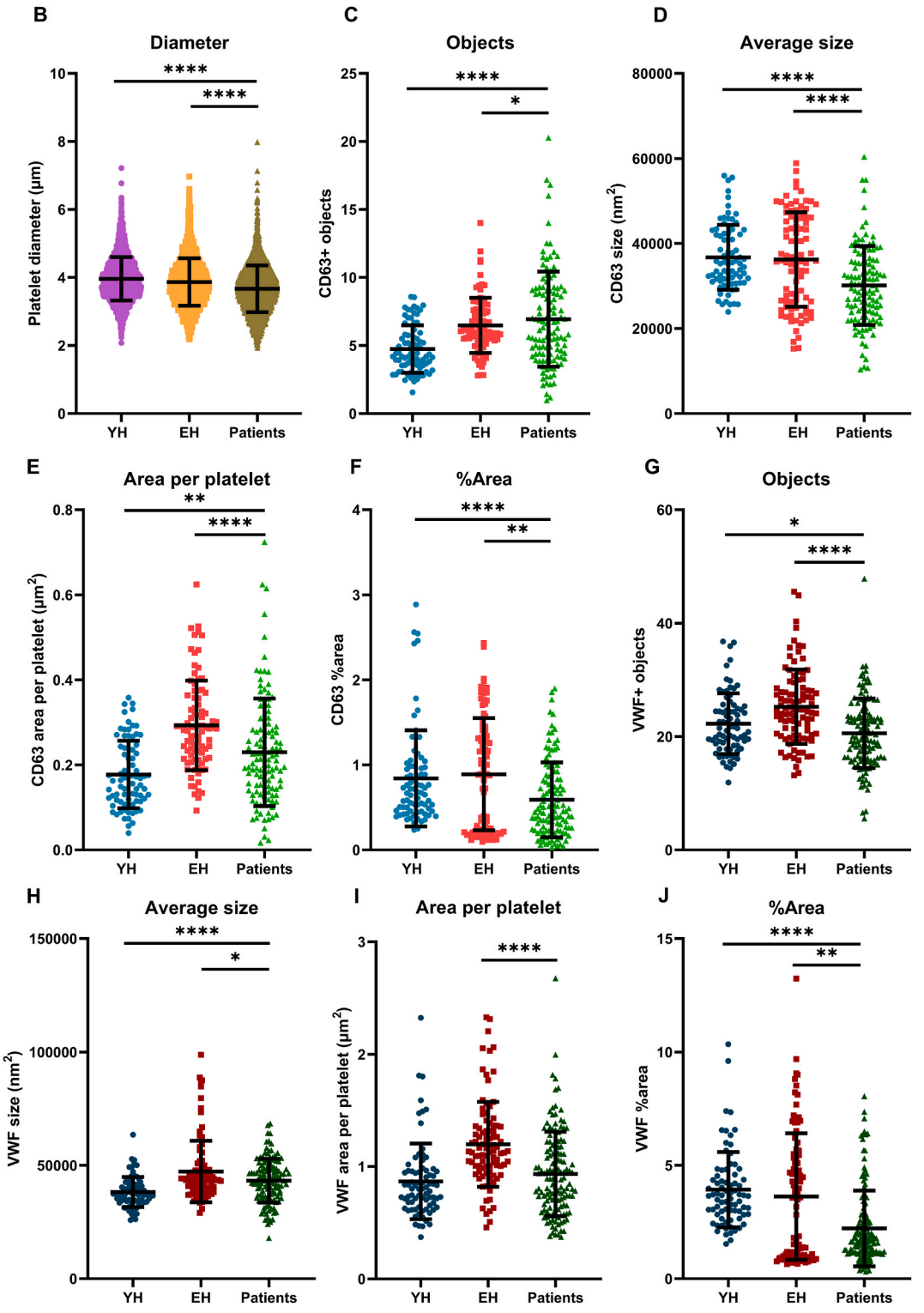

Fig. 2. (*continued*).

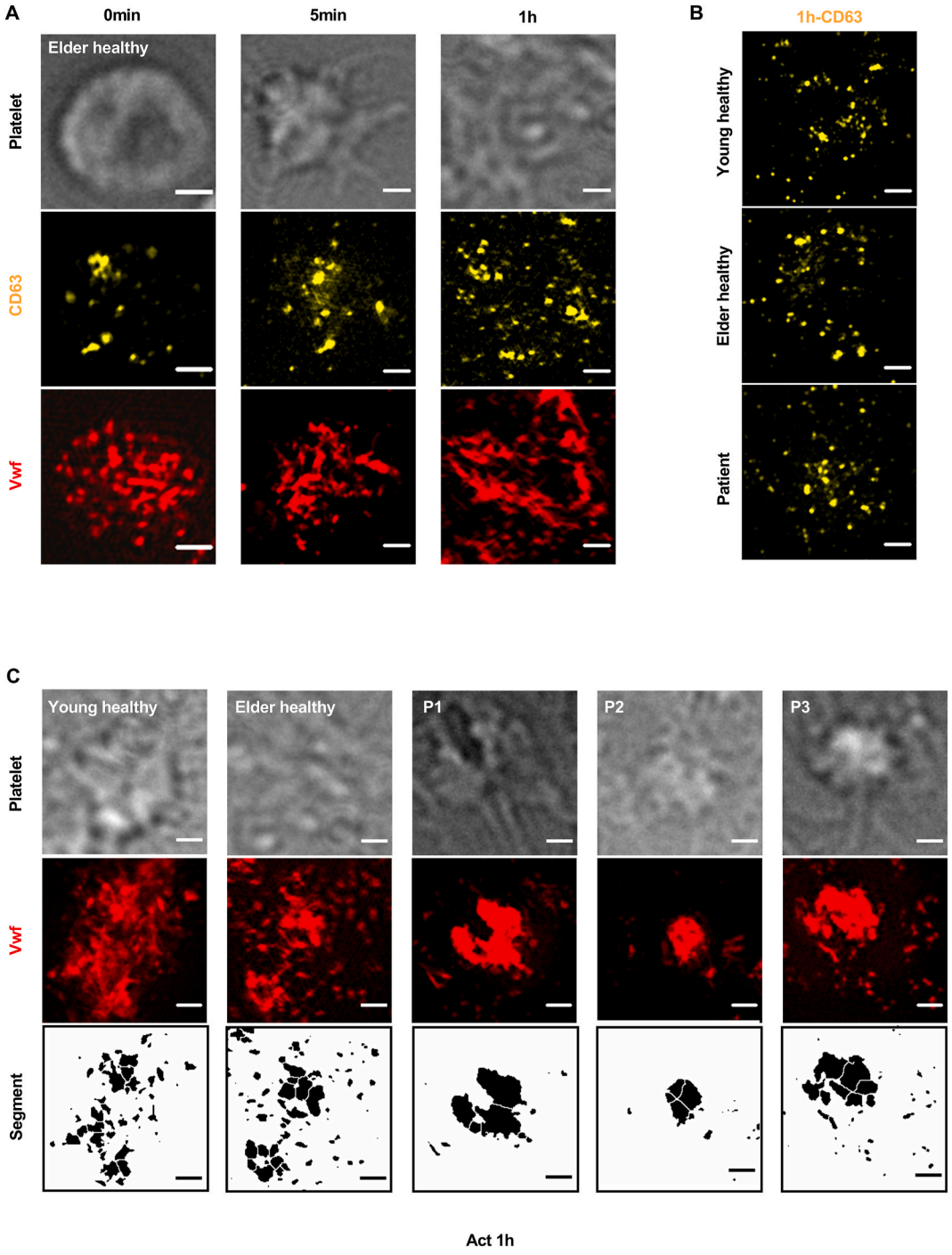

Fig. 3. α-granule in AIS patients displayed parenchymal-like fluorescent blocks under thrombin stimulation. A, SIM images of platelet activated by 0.5U TH after 0min, 5 min and 1 h from one health control (n = 6). CD63 (yellow) showed no significantly difference in morphology at different time point. VWF (red) aggregation increased over time and presented honeycomb-like block in 1 h. **B**, CD63 showed no difference between YH, EH and AIS patient (n = 3) after 1 h stimulation. **C**, VWF altered to parenchymal-like fluorescent block in AIS patients (n = 3) while health people (n = 6) presented honeycomb-like block after 1 h stimulation. The bottom row was segmentation diagram of VWF, indicating VWF in AIS patients was difficult to be segmented. Scale bar:1 μm. **D**, VWF area greater than the upper limit of the resting group was defined as large VWF. Large VWF number was less in AIS patients than controls. **E**, Large VWF was divided into 7 different ranges according to number. The pie chart showed proportion of total image amount in each range. (For interpretation of the references to color in this figure legend, the reader is referred to the Web version of this article.)

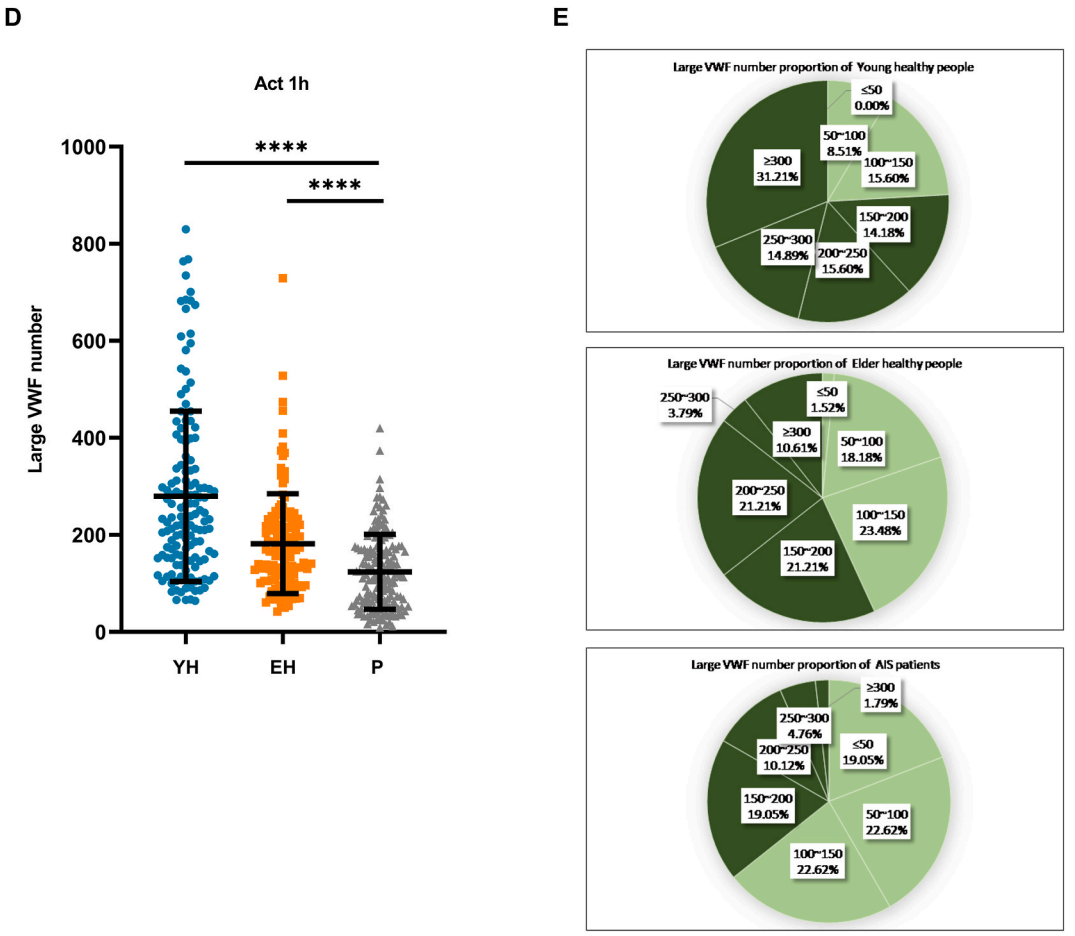

Fig. 3. (*continued*).

3.2. Quantitative imaging of platelet diameter and granule content

We used immunofluorescence to label CD63 of dense granules and VWF of α-granules. Quantitative analysis refers to converting the image information of SIM into digital information in order to obtain the numerical value of each platelet as well as its ultrastructure for analysis, which in our study is dense granule and α-granule. This conversation benefits from the high resolution of SIM, which could clearly capture the granules inside the platelets. In addition to measuring platelet diameter, we also analyzed CD63 dots, average CD63-positive dots area, CD63-positive area per platelet, CD63-positive area Fov, VWF dots, average VWF-positive dots area, VWF-positive area per platelet and VWF-positive area Fov from 7162 platelets in rest group. The number of Stained CD63 dots or VWF dots measured in single platelets are denoted as $CD63^+$ objects or VWF + objects. Although no visual morphological differences in rest platelets were observed, we finally found platelet size and ultrastructure included CD63 and VWF changed significantly in AIS patients after quantitative analysis.

Our quantification showed that the platelet diameter was shorter in AIS patients than controls (YH vs $P = 3.96 \pm 0.64$ μm vs 3.67 ± 0.69 μm, $P < 0.0001$; EH vs $P = 3.87 \pm 0.70$ μm vs 3.67 ± 0.69 μm, $P < 0.0001$; Fig. 2B). Totally 7162 platelets from 11 patients with AIS and 12 controls (EH and YH) were calculated for comparison through SIM images (Fig. 2B). The Mann-Whiyney test results showed that the mean platelet diameter in elder healthy control was significantly shorter than that in young healthy control (YH vs $EH = 3.96 \pm 0.64$ μm vs 3.87 ± 0.70 μm , $P < 0.0001$). Although mean platelet diameter decreased with age, it was the shortest in AIS patients.

All measurements were lower in AIS patients than in healthy individuals except $CD63^+$ objects. $CD63^+$ objects were significantly increased in AIS patients (YH vs $P = 4.7 \pm 1.7$ vs 6.9 ± 3.5, $P < 0.0001$; EH vs $P = 6.48 \pm 2.03$ vs 6.9 ± 3.5, $P = 0.0213$; Fig. 2C). CD63 size represents average CD63-positive dots area, which decreases with age and is more pronounced in AIS patients (YH vs $P = 36732.54 \pm 7626.26$ nm^2 vs 30123.31 ± 9279.02 nm^2, $P < 0.0001$; EH vs $P = 36247.86 \pm 11109.54$ nm^2 vs 30123.31 ± 9279.02 nm^2, $P < 0.0001$; Fig. 2D). In contrast to the decrease of single stained CD63 size with age, CD63-positive area per platelet which we named CD63 area per platelet increased instead (YH vs $EH = 0.177 \pm 0.08$ μm^2 vs 0.29 ± 0.11 μm^2, $P < 0.0001$; Fig. 2E). However, they fell back again when people suffered an AIS (EH vs $P = 0.29 \pm 0.11$ μm^2 vs 0.23 ± 0.13 μm^2, $P < 0.0001$; Fig. 2E). When calculating CD63-positive area Fov, namely CD63 %area, this value was found to decrease more significantly in AIS patients, even lower than YH (YH vs

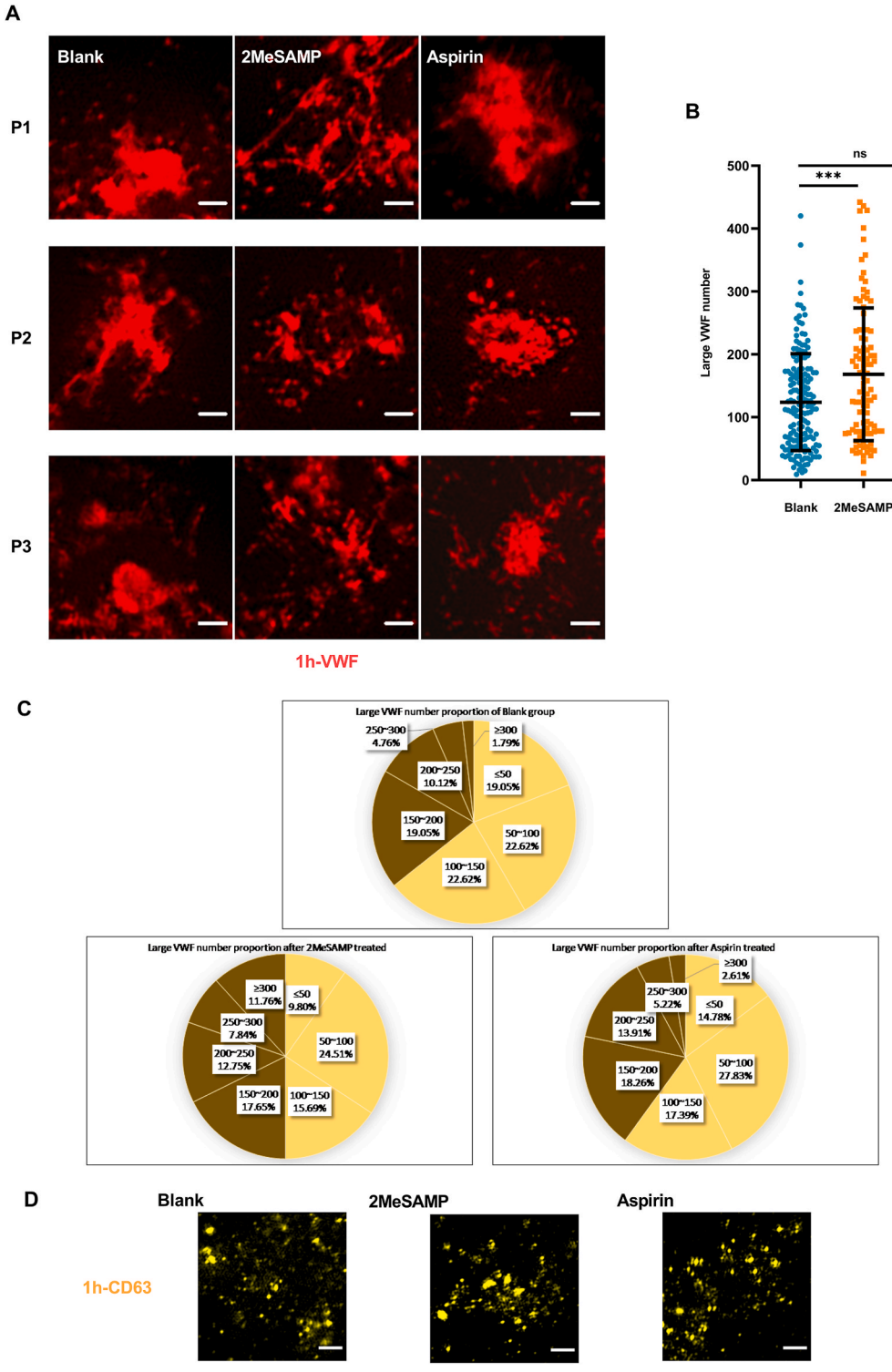

Fig. 4. 2MeSAMP depolymerized parenchymal-like fluorescent blocks of α-granule. A, SIM image of platelet VWF (red) from 3 AIS patients. Under 0.5U TH stimulation, ACDT administrated in column 1, 2MeSAMP administrated in column 2, Aspirin administrated in column 3. The results showed 2MeSAMP depolymerized parenchymal-like fluorescent block of VWF in α-granule. And aspirin didn't influence the fluorophores formation of α-granule. **B**, Large VWF number decreased after 2MeSAMP treated, no effect in Aspirin group. **C**, Proportion of total image amount in 7 different range for blank group, 2MeSAMP group and Aspirin group. **D**, Platelet CD63 (yellow) morphology had no obvious change under different treatment. Scale bar:1 μm. (For interpretation of the references to color in this figure legend, the reader is referred to the Web version of this article.)

P = 0.84 ± 0.57 vs 0.59 ± 0.44, P < 0.0001; EH vs P = 0.89 ± 0.66 vs 0.59 ± 0.44, P = 0.0074; Fig. 2F).

All quantitative measurements of VWF showed a trend of becoming larger with age and decreasing again in patients with AIS. VWF + objects were significantly reduced in AIS patients and even lower when ompared to YH (YH vs P = 22.27 ± 5.36 vs 20.57 ± 6.14, P = 0.0418; EH vs P = 25.23 ± 6.53 vs 20.57 ± 6.14, P < 0.0001; Fig. 2G). Instead, VWF size decreases in AIS patients but not less than the value in YH group (YH vs P = 38240.24 ± 6629.57 nm^2 vs 43237.12 ± 9681.11 nm^2, P < 0.0001; 47246.50 ± 13530.28 nm^2 vs 43237.12 ± 9681.11 nm^2, P = 0.0107; Fig. 2H). The same trend of VWF area per platelet was showed between the patients and the healthy controls. The difference was that the VWF area per platelet of patients decreased to similar levels to the YH group (YH vs P = 0.87 ± 0.34 μm^2 vs 0.93 ± 0.38 μm^2, P = 0.1693; EH vs P = 1.20 ± 0.38 μm^2 vs 0.93 ± 0.38 μm^2, P < 0.0001; Fig. 2I). In the quantitative analysis of VWF, the only decrease data with age was VWF %area, and this reduction was more obvious in AIS patients (YH vs P = 3.93 ± 1.66 vs 2.22 ± 1.67, P < 0.0001; EH vs P = 3.63 ± 2.79 vs 2.22 ± 1.67, P = 0.0099; Fig. 2J).

3.3. VWF in AIS patients changed to parenchymal-like fluorescent blocks after stimulation of TH

0.5U thrombin (TH) was given to healthy controls and patients with AIS to stimulate the platelets, and SIM was used to observe

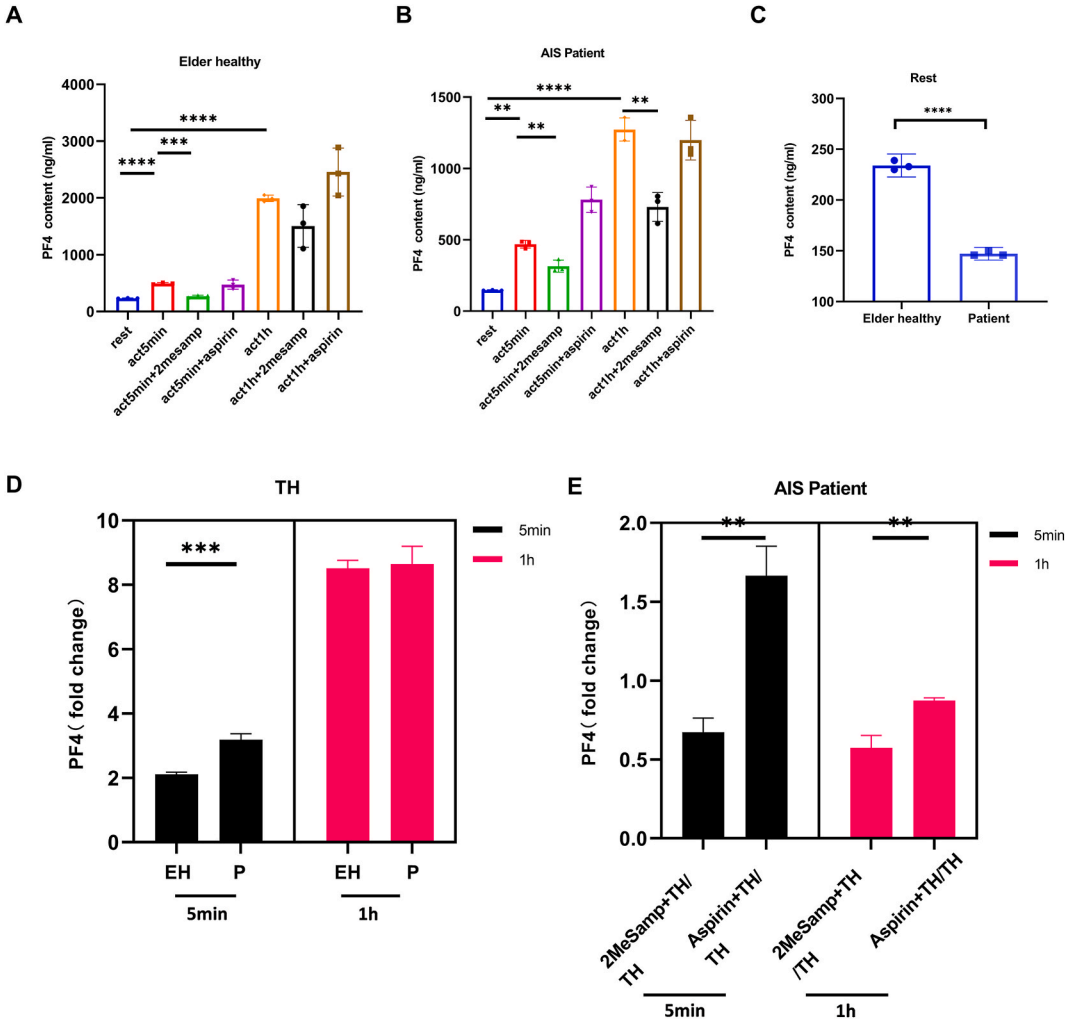

Fig. 5. PF4 content was lower in AIS patient but release more after being stimulated while 2MeSAMP inhibited PF4 releasing. A, PF4 content of elder healthy in 7 different groups (n = 3). PF4 release increased after 5 min and 1 h of thrombin stimulation (****P < 0.0001; ****P < 0.0001). Releasing of PF4 decreased after dealing with 2MeSAMP for 5 min and 1 h (***P = 0.0001). **B**, PF4 content of AIS patients in 7 different groups (n = 3). PF4 release increased after 5 min and 1 h of thrombin stimulation (****P < 0.0001; ****P < 0.0001). Releasing of PF4 decreased after dealing with 2MeSAMP for 5 min and 1 h (**P = 0.0062; **P = 0.0019). **C**, PF4 content was lower in AIS patients (n = 3) at rest stage (****P < 0.0001). **D**, Ratio of PF4 content after activation to before. Stimulated with 0.5U TH for 5 min, the ratio was higher in AIS patients (n = 3) compared with EH (n = 3) (***P = 0.0007). **E**, Ratio of PF4 content after drug administration to before. The ratio was lower after treatment with 2MeSAMP for 5 min and 1 h compared with aspirin (**P = 0.0012; **P = 0.003). Unpaired two-tailed Student's t-test. Data are presented as Mean value standard deviation.

morphological changes in platelets, CD63 in dense granules, and VWF in α-granules at times of 0 min, 5 min, and 1 h (Fig. 3A). Within 5 min stimulation of platelets, they began to spread out and extend pseudopodia from the disk. VWF gradually aggregate into large VWF (the area was larger than the highest area in rest state) and adhere to one another in both healthy individuals and patients with AIS (Fig. 3A, S1). After activation for 1 h, multiple platelets are gathered together to form blood clots (Fig. 3A). We didn't observe obvious change in the morphology of CD63 at 0 min, 5 min and 1 h after thrombin activation (Fig. 3B). At 1 h time point, in contrast to healthy people, AIS patients showed morphological differences in VWF. In patients with AIS, visually observed VWF accumulated together forming denser fluorophores with little gap and few diffuse particles around VWF, thus making them difficult to segment visually (Fig. 3C). We calculated the large VWF number of activated platelets in each image. The large VWF number was less in AIS patients compared with healthy controls ($P_{YH\ VS\ P} < 0.0001$; $P_{EH\ VS\ P} = 0.0002$; Fig. 3D). Large VWF was divided into 7 different ranges according to number. Proportion of total images in each range was made into a pie chart (Fig. 3E). Subsequently, we defined Honeycomb-like block and Parenchymal-like block according to the proportion of images of large VWF number over 150. When the proportion of images of large VWF over 150 was more than 50%, the VWF aggregation was defined as Honeycomb-like block. On the contrary, it was defined as Parenchymal-like block. Honeycomb-like means looser adhesion of VWF which has more amount of large VWF. Parenchymal-like means denser adhesion of VWF with fewer amount of large VWF. It was evident that 33.93% images of AIS patients with a large VWF count over 150, clustered into Parenchymal-like block. Compared with AIS patients, the large VWF clustered into Honeycomb-like block in health controls whose the proportion of images with a large VWF count over 150 was higher, accounting for 75.88% in young healthy and 56.82% in elder healthy respectively.

3.4. VWF parenchymatous fluorescent blocks were inhibited by 2MeSAMP

The antiplatelet drugs 2MeSAMP and Aspirin inhibit the ADP receptor and COX-1 receptor, respectively. 10 μM 2MeSAMP and 53 μM Aspirin were administered to AIS patients' platelets in vitro, respectively, before activating with 0.5U TH for 1 h. After 2MeSAMP treatment, more single platelets were observed in the wide field than after ACDT (blank) or Aspirin treatment (S2). It could be visually observed that parenchymal-like fluorescent block morphology of large VWF in patients was suppressed in response to 2MeSAMP treatment (Fig. 4A). Meanwhile, large VWF could be segmented easily. No morphology changes of large VWF were observed visually after treated with Aspirin. The number of large VWF increased after treated with 2MeSAMP ($P = 0.0008$; S2). With Aspirin treatment, there was no statistically significant increase in large VWF amount ($P = 0.1963$). When treated with 2MeSAMP, the proportion of images with a large VWF count over 150 increased from 33.93% to 50% (Fig. 4). At the same time, the proportion increased from 33.93% to 40% after treated with Aspirin. This phenomenon showed that 2MeSAMP had a stronger effect on inhibiting the formation of parenchymal-like fluorescent block morphology of VWF in AIS patients. When 2MeSAMP inhibition was used, it was obvious that VWF changed from denser parenchymal-like fluorescent block to looser honeycomb-like block, which suggested that parenchymal-like fluorescent block represented the greater function of platelet α-granules. Observations of CD63 in dense granules did not reveal obvious morphological changes (Fig. 4B, S3).

3.5. AIS patients had a higher level of PF4 and 2MeSAMP inhibited PF4 release

A protein factor called PF4 is released from α-granules. As platelets of AIS patients and healthy controls were observed to have VWF structurally changed after activation, PF4 was detected in their supernatants. The supernatants were from different state (resting, 0.5U TH activation or 0.5U TH activation after inhibitor treatment) in AIS patients and healthy controls. In the rest stage, PF4 releasing in the AIS group was significantly lower than in the healthy group (EH vs $P = 233.953 \pm 4.587$ ng/ml vs 147.152 ± 2.514 ng/ml, $P < 0.0001$; Fig. 5C). PF4 levels in EH were 233.953 ± 4.587 ng/ml at rest, 493.772 ± 16.271 ng/ml after 5 min of activation and 1992.247 ± 57.766 ng/ml after 1 h of activation, respectively (Fig. 5A). PF4 levels in AIS patients were 147.152 ± 2.514 ng/ml at rest, 468.824 ± 27.016 ng/ml after 5 min of activation and 1272.477 ± 80.908 ng/ml after 1 h of activation, respectively (Fig. 5B). Due to the heterogeneity of platelets in individuals, direct comparisons of the release of PF4 during activation are not reasonable. Therefore, in AIS patients and healthy controls, platelet activation release was normalized by comparing fold change in PF4 release before and after activation. In patients and healthy subjects, the fold change of PF4 release after 5 min and 1 h activation were (EH vs $P = 2.111 \pm 0.070$ vs 3.186 ± 0.184, $P = 0.0007$; Fig. 5D) and (EH vs $P = 8.516 \pm 0.247$ vs 8.647 ± 0.550, $P = 0.724$; Fig. 5D). The PF4 release after inhibitors' treatment except for that ACDT (platelet storage solution) treatment to obtain the inhibitory effect of the drugs on platelet release. No matter activated for 5 min or for 1 h, 2MeSAMP inhibited PF4 release more effectively than Aspirin (PF4 fold change 5 min: 2MeSAMP vs Aspirin $= 0.672 \pm 0.091$ vs 1.665 ± 0.091, $P = 0.0012$; 1 h: 2MeSAMP vs Aspirin $= 0.573 \pm 0.079$ vs 0.875 ± 0.016, $P = 0.003$; Fig. 5E). PF4 concentrations in supernatants of AIS patients and healthy controls differed depending on the state. First, in the resting state, PF4 of supernatant in patients are lower than that in healthy individuals. However, in the activated state, PF4 fold change increased more in patients' supernatant than in healthy subjects. Finally, the reduction of PF4 fold change in the supernatant reduced more pronounced after treatment with 2MeSAMP.

4. Discussion

Structured Illumination Microscopy (SIM) is a new imaging technique which uses immunofluorescence to label ultrastructure of cells. The SIM has several advantages, such as precise observation with high resolution, less sample damage, and easier imaging than conventional techniques. The imaging mode of SIM during the acquisition of sample images can extract high frequency information which can't acquire normally by computer and reconstruct images [31,32]. Since SIM has a high resolution, it is well suited for

observing the platelet sample with only 150 nm ultrastructure [23]. Today, SIM technique is applicable to novice microscopists with increasingly easy-to- operate commercial system. Despite there are so many advantages, SIM still has some shortcomings. More than anything, only doubled improved resolution means that SIM need brighter fluorescent dyes or more intense laser power to acquire high quality images [33,34]. High laser energy will increase photobleaching and shorten the life of laser device. To overcome the limitation, bright and stable dyes of samples are required. Extremely small molecular structure and lacking of suitable and stable dyes limit the application of SIM [35]. On the other hand, noise is inevitable in fluorescence microscopy imaging [36]. Design of SIM and reconstruction method could improve the signal-to-noise ratio to some extent. Although the operation of SIM is much simpler and easier than that of the electron microscope, as an optical instrument, non-professionals still need to be trained in the instrument before using SIM. Besides, the assembly of the SIM requires a large sum of money. These limitations may affect widely adoption of SIM. In the future, we could try to establish a SIM regional center to send all samples to the center for testing, in order to reduce the human and financial costs of using SIM to evaluate platelets in AIS patients. Considering the advantages and disadvantages of SIM, in the cases of SIM providing sufficient resolution it may prove advantageous over other super resolution techniques [36]. CD63 and VWF are abundant in dense and α-granules with stable antibodies, which make them suitable for platelet analyzing of SIM. In the disease associated with platelet granules deficiency, the researchers applied SIM to directly observe a decrease in platelet granules in patients [29,37]. Some papers have also proposed applying SIM to the diagnosis of kidney disease and cancer [28,38,39]. These studies provided references for us to study granule changes of platelets in AIS patients.

This study successively assessed morphology, number and area of platelet dense granules and α-granules in AIS patients through SIM technique. Previous studies using electron microscopy to observe platelets in AIS patients have showed that the number of α-granules were reduced in AIS patients [40,41]. This study exhibited the same results by SIM. In addition, the results showed the area of α-granules also decreased and the number of platelet dense granules was increased and the area was decreased in AIS patients compared with controls, which hasn't informed before. VWF is a protein stored in α-granules that releases after platelet activation. Platelet VWF releases to plasma will result in the VWF number decreased in AIS patients. Two independent case-control studies (COCOS and ATTAC) verified that plasma VWF level elevated in AIS patients and increased secretion of VWF may be the pathogenesis of AIS [42]. The decreased area of platelet VWF may be beneficial for secreting. Released VWF mediates platelet adhesion to endothelium and activates local platelet, which is the first step of AIS. Unfortunately, the function of increased number and decreased area of CD63 of dense granule in AIS is still not clearly. Platelet α-granules aggregated with thrombin stimulation particularly in AIS patients whose α-granules aggregated into Parenchymal-like block with lower large VWF amount and harder to segment than controls. Such significantly differentiation in AIS patients after stimulating by agonist is not surprising because they already abnormal in rest state. Dramatic morphology change of α-granules in AIS patients means functional differences in α-granules between AIS patients and controls which could be confirmed by PF4 release test after activation. The formation of Parenchymal-like block in α-granules of AIS patients was inhibited after treatment with P_2Y_{12} receptor antagonist, which indicated that Parenchymal-like block represented stronger activation state. Hence, formation of Parenchymal-like block of α-granules in AIS patients correlated with hyper-responsiveness to stimulus. Surprisingly, there were no significantly morphology changes in α-granules of AIS patients before and after COX-1 inhibitor treatment. P_2Y_{12} receptor antagonist inhibited the formation change of α-granules while COX-1 inhibitor didn't. This differ may link to different mechanism or antiplatelet effects of the two drugs. The study indicated that there were significant changes in morphology, number and area of platelet granules in AIS patients. And the morphology changes could be suppressed by P_2Y_{12} receptor antagonist. By the way, the results also showed that number and area in platelet granules changed with age in healthy subjects and the tendency was similar to AIS patients. But morphology changes of platelet granules haven't found with age. Moreover, the differences of number and area in platelets were still existed between AIS patients and elder healthy subjects. In other words, age will affect the number and area of platelet granules to a certain extent, which is not enough to cause morphology changes of platelet granules. However, in the disease state of AIS, platelet granules continue to change on the basis of the age. Such changes of platelet granules not only reflect in the number and area, but also in the morphology. Therefore, to avoid the influence of age, it would be more reliable to compared patients with elder healthy subjects. If there were increased number and decreased area of dense granules, decreased number and area and Parenchymal-like block formation of α-granules when compared patients with elder healthy subjects, there would be a high risk of AIS. The risk of AIS would further increase if patients suffered neurological deficit symptoms recently such as transient dizziness or limb numbness.

For the analysis of CD63 in dense granules and VWF in α-granules, they all showed significantly differences between AIS patients and healthy subjects. From the results of the study, VWF showed significant changes in number, area as well as morphology and CD63 showed no morphology changes. Endothelia cells (EC) and megakaryocytes synthesize VWF, a large multimeric glycoprotein [43]. Mature VWF from EC is stored in Weibel-Palade bodies (WPB) or partially released and those from megakaryocytes are stored in α-granules of platelet [44]. There are some differences between plasma VWF and platelet VWF. Plasma VWF bridges platelet adhesion to the vessel wall through GPIb and activates platelets locally. Activated platelets release platelet VWF, which promotes hemostasis and thrombosis by binding to GPIIb/IIIa complex enhancing platelet spreading and aggregation. However, platelet VWF doesn't release to plasma all the time. When the stimulus is weak, α-granules release platelet VWF which almost expressed on platelet with slightly elevated in plasma. Even though stimulated with strong agonist, platelet VWF also preferentially binds to GPIIb/IIIa on the platelet surface and released into plasma subsequently [45]. Epinephrine induces EC release VWF by increasing concentration of cAMP and calcium under stress without releasing of platelet VWF [46]. This means different releasing mechanism of VWF in platelets and VWF in EC. The plasma VWF level increases during many pathophysiological stimuli such as pregnancy, atherosclerosis, tumor and inflammation. During acute phase of vascular perturbation, plasma VWF level increases and gradually decreases at later time points. On the contrary, level of plasma VWF consecutively increases when the periods of vascular diseases extended [47]. It has been demonstrated that these elevated plasma VWF were from EC [48], but VWF released from activated platelets can't be ruled out. Both

VWF and *P*-selection plasma level increased in AIS patients. *P*-selection is a marker of platelet activation released from α-granules by activated platelet. Along with the releasing of contents in α-granules, platelet VWF secrets at the same time according to its releasing characteristic. Therefore, when the release of *P*-selection increases, it is accompanied by the release of platelet VWF. It's suggested that platelet VWF is also partially released into plasma in AIS patients and the elevated plasma VWF is the result of co-release of EC and α-granules. Thus, the decreased number of platelet VWF in AIS may be related to the increased release.

Circulating ultra large VWF (ULVWF) which is more adhesive than small multimers is segmented to smaller forms by ADAMT13 (a disintegrin and metalloproteinase with a thrombospondin motif repeats 13) at the Tyr1605-Met1606 site in A2 domain to cleave [49], which finished in several seconds to minutes. When the ADAMT13 is lacking in vivo, as in Thrombotic Thrombocytopenic Purpura (TTP) disease, the clearance time and amount of VWF are abnormal, leading to microvascular thrombosis and organ ischemic infraction [50]. Prospective population-based cohort studies have revealed that low plasma ADAMT13 levels are related to risk and poor outcomes in AIS [51,52]. These studies suggested that both decreased amount of ADAMT13 and abnormal microenvironment would affect ULVWF elimination. Alternatively, reduced sialic acid on *N*-linked glycans of platelet VWF may be associated with ADAMT13 resistance, indicating that glycosylation composition of VWF also reduced the sensitivity of ADAMT13 [53]. Platelet VWF of AIS patients aggregated into denser Parenchymal-like block than controls. The mechanism of abnormal aggregation of VWF in AIS patients could be either the hyperresponsiveness of platelets or decreased clearance of large VWF. Lower ADAMT13 activity resulted from abnormal synthesis or abnormal functional microenvironment will reduce clearance of large VWF after platelet activation in AIS patients. It is also possible that there is a genetic mutation of platelet VWF during synthesis in AIS patients. The altered structure of VWF is resistance to ADAMT13, reducing the degradation of VWF and thus forming tighter clumps than that in controls. In summary, the decreased number and area of VWF in AIS patients and the abnormal morphology after being stimulated by thrombin may be related to the following reasons: (1) more platelet VWF released to plasma; (2) increased plasma VWF levels; (3) abnormal synthesis and functional environment of ADAMT13; (4) abnormal mutations during VWF synthesis causing ADAMT13 resistance. These mechanisms may exist singly or simultaneously leading to abnormal platelet structure in AIS patients before onset, further influencing the morphology and function of platelets, and mediating the occurrence and development of AIS eventually.

In recent years, researchers believe that the interaction between platelets and neutrophils is related to the occurrence and progression of AIS [54,55]. Activated platelet can release a large number of chemokines such as CXCL4 (platelet factor 4, PF4) , CXCL4L1 and CCL5 to recruit monocytes and mediate inflammatory. These chemokines released by activated platelet are shown to accelerate the process of atherosclerosis and result in AIS or acute coronary syndrome eventually (ACS). The assay tested PF4 by ELISA has illustrated that PF4 level elevated 3 folds in ACS [56]. This means platelet activated and released more PF4 to plasma in ACS. Therefore, we supposed that PF4 level can also reflect platelet release function in AIS to some extent.

The assay tested plasma PF4 level proved that PF4 elevated in AIS patients [57]. However, our experiment detected decreased PF4 in AIS patients. The opposite results may be related to the PF4 content of washed platelets compared to previous measurements of plasma PF4 content. Interestingly, the higher release rate of PF4 in AIS patients after thrombin stimulation indicated that platelets in AIS patients have higher reactivity. This result again confirmed that the denser VWF aggregation observed by SIM in AIS patients represented hyperresponsiveness to stimulus. The mechanism of PF4 in AIS is to promote atherosclerosis and thrombo-inflammation. For the former, PF4 recruits monocytes by depositing PF4 and CXCL5 on EC and monocyte [58], exacerbates atherosclerosis through increasing uptake of oxidized low density lipoproteins (ox-LDL) by macrophages [59], downregulates athero-protective receptor CD163 by inducing differentiation of macrophages [60]. For the later, PF4 promotes differentiation of regulatory T cells (Treg's) of α/CD63cd28-stimulated CD4 + T cell. The more significant increase of platelet PF4 after stimulation in AIS patients indicated that there will be a more sever inflammatory response [61]. The assay injecting the PF4-CCXL5 isomer inhibitor MKEY reduced macrophage infiltration as well as the infarction area after stroke supported this hypothesis [62]. Our findings on activated platelets found that platelets from AIS patients are hyperresponsive after stimulation. The platelet ultrastructure alteration reflects not only the SIM-based ultrastructure alteration but also the ELISA-based more powerful release function. Hyperactivity and hyperresponsiveness mean as administrated to the same degree of stimulation, AIS patients have more easily activated platelets and more tightly bound α-granules than healthy individuals. Previous studies also support the conclusion [63,64]. Therefore, we speculate that platelets in patients with AIS are more likely to aggregate as well as adhering than platelets in healthy individuals when platelets are stimulated.

Antiplatelet drug 2MeSAMP inhibits the hyperresponsiveness of platelets in AIS patients. 2MeSAMP is an ADP receptor antagonist with in vitro activity, which could depolymerize activated platelets α-granules from a pattern of parenchymal-like fluorescent blocks to honeycomb-like block in AIS patients (Fig. 4A). Conversely, when treated with COX-1 inhibitor named Aspirin, did not significantly change the morphology of α-granules. Antagonists for P2Y12 receptors and inhibitors for COX-1 are commonly used antiplatelet drugs in AIS patients [65]. Although widely used, there are currently no relevant selection standards. There is currently lack of direct visualization observation on effect of platelet ultra-structures of antiplatelet drugs. This study filled this gap with SIM technique. Activated platelets release ADP binding to receptor P_2Y_1 or P_2Y_{12}. After that, integrin GPIIb/IIIa could be activated through $G_{\beta\gamma}$-PI3K-Rap 1 pathway [66]. Binding of Platelet VWF and GPIIb/IIIa amplify and stabilize platelet aggregation [67]. Treated with P_2Y_{12} receptor antagonist affected the activation of GPIIb/IIIa, subsequent inhibiting the binding between platelet VWF and GPIIb/IIIa. This may be the mechanism by which platelet VWF parenchymal-like fluorescent blocks was inhibited after treatment with P_2Y_{12} receptor antagonist. The study has shown that Aspirin treatment didn't affect the platelet VWF expression after thrombin stimulated [44]. We also didn't find effect of Aspirin on the morphology of platelet VWF by SIM. Besides, treatment with 2MeSAMP decreased PF4 release from α-granules, but not with Aspirin. This is consistent with the results of a vivo assay in which PF4 level didn't change in ACS patients received Aspirin treatment (i.v.) [56]. However, another experiment indicated that both Aspirin and cangrelor (P_2Y_{12} receptor inhibitor) decreased the level of PF4 [68]. There may be two reasons for the different results. Firstly, the sample of later experiment was from healthy individuals without cardiovascular or cerebrovascular diseases. Secondly, Aspirin had a longer duration

of action (subjects took Aspirin orally one day in advance) in the later assay. Our experimental conditions are more similar to the former one and the results were consistent. When ADP binds to P_2Y_{12} receptor, release of α-granules will upregulate through $G_{\alpha i2}$-AC-cAMP-PKC pathway [66,69]. This can explain the lower PF4 release after P_2Y_{12} receptor antagonist treated. Actually, after prolonged Aspirin treatment, PF4 release was partially inhibited. The mechanism is not clearly, may be an inhibition of platelet activation. Significant impact on morphology and function of α-granules might represent a more powerful inhibitory effect of P_2Y_{12} receptor antagonist. It has been reported that P2Y12 receptor antagonists provide a better protection for patients with coronary heart disease or AIS than COX-1 inhibitors in several clinical studies [70,71]. The mechanism may be additional anti-atherosclerotic and neuroprotective effects of P_2Y_{12} receptor antagonists besides inhibiting platelet aggregation [72–74]. We visually observed the effect of P_2Y_{12} receptor antagonists on α-granules morphology directly through SIM technique. In addition, release factors detected also reflects the inhibitory effect of P_2Y_{12} receptor antagonists on platelet function. These indicate that SIM has the ability to distinguish the effects of different drugs on platelet structure. And the results suggested that P_2Y_{12} receptor antagonists may be a better choice for secondary prevention after AIS.

5. Conclusion

Despite the important role platelets play in AIS disease, further knowledge is needed about the details of platelet ultrastructure and how it changes in patients with AIS. Furthermore, in the later stages of AIS, whether to use a P2Y12 receptor antagonist or a COX-1 inhibitor of AIS remains controversial. Based on SIM observation, we found that platelets in AIS patients have heterogeneous ultrastructure whether they are at rest or activated state. Otherwise, 2MeSAMP is more powerful than aspirin at inhibiting granule formation in vitro. Our experiments complement SIM-based information on platelet ultrastructure in patients with AIS and can provide a reference for future related studies. This study provides a new perspective on the pathogenesis of AIS and the mechanism of antiplatelet drugs. SIM analysis of platelet ultrastructure may offer a new method of detecting AIS and antiplatelet drugs in the future.

Funding

Fund for Knowledge Innovation of Wuhan Science and Technology Bureau (Grant No.2022020801010558). Fund for Special fund for Young Backbone talents of Wuhan Fourth Hospital. This work also supported by the Medical Research Project of Wuhan Municipal Health Commission (Grant No. WG14B13), The National Natural Science Foundation of China (Grant No. 31600692), and the Natural Science Foundation of Hubei Province (2017CFB406).

Ethical approval

The study had acquired ethic approval through Wuhan Forth Hospital and the approval number was Lun Shen Zi (KY2021-086-01). All research was performed in accordance with relevant guidelines and regulations. All the volunteers signed informed consent forms.

Data availability

All data generated or analyzed during this study are included in this published article (and its Supplementary Information files).

Declaration of competing interest

The authors declare that they have no known competing financial interests or personal relationships that could have appeared to influence the work reported in this paper.

Acknowledgements

We thank all the volunteers for their participation in the study. The authors thank Huan Deng and Qian Jiang for assisting in laboratory equipment. And we thank all other staff at neurology department in Wuhan Puai Hospital for help collecting samples, as well as blood transfusion laboratory of Wuhan Blood Center for supplying equipment.

Appendix A. Supplementary data

Supplementary data to this article can be found online at https://doi.org/10.1016/j.heliyon.2023.e18543.

References

[1] regional Global, regional, and national, and national burden of neurological disorders during 1990-2015: a systematic analysis for the Global Burden of Disease Study 2015, Lancet Neurol. 16 (11) (2017) 877–897.
[2] D.A. Rubenstein, W. Yin, Platelet-activation mechanisms and vascular remodeling, Compr. Physiol. 8 (3) (2018) 1117–1156.

[3] H.P. Adams Jr., et al., Classification of subtype of acute ischemic stroke. Definitions for use in a multicenter clinical trial. TOAST. Trial of Org 10172 in Acute Stroke Treatment, Stroke 24 (1) (1993) 35–41.
[4] W. Herrington, et al., Epidemiology of atherosclerosis and the potential to reduce the global burden of atherothrombotic disease, Circ. Res. 118 (4) (2016) 535–546.
[5] S.P. Jackson, Arterial thrombosis–insidious, unpredictable and deadly, Nat. Med. 17 (11) (2011) 1423–1436.
[6] K.M. Meyers, H. Holmsen, C.L. Seachord, Comparative study of platelet dense granule constituents, Am. J. Physiol. 243 (3) (1982) R454–R461.
[7] R.M. Camire, et al., The mechanism of inactivation of human platelet factor Va from normal and activated protein C-resistant individuals, J. Biol. Chem. 270 (35) (1995) 20794–20800.
[8] H. Hartwig, et al., Platelet-derived PF4 reduces neutrophil apoptosis following arterial occlusion, Thromb. Haemostasis 111 (3) (2014) 562–564.
[9] R.R. Koenen, et al., Disrupting functional interactions between platelet chemokines inhibits atherosclerosis in hyperlipidemic mice, Nat. Med. 15 (1) (2009) 97–103.
[10] S. Sharma, T. Tyagi, S. Antoniak, Platelet in thrombo-inflammation: unraveling new therapeutic targets, Front. Immunol. 13 (2022), 1039843.
[11] J. Rayes, et al., The dual role of platelet-innate immune cell interactions in thrombo-inflammation, Res. Pract. Thromb. Haemost. 4 (1) (2020) 23–35.
[12] M. Pawelczyk, B. Kaczorowska, Z. Baj, The impact of hyperglycemia and hyperlipidemia on plasma P-selectin and platelet markers after ischemic stroke, Arch. Med. Sci. 13 (5) (2017) 1049–1056.
[13] F. Rendu, B. Brohard-Bohn, The platelet release reaction: granules' constituents, secretion and functions, Platelets 12 (5) (2001) 261–273.
[14] S. Raghunathan, J. Rayes, A. Sen Gupta, Platelet-inspired nanomedicine in hemostasis thrombosis and thromboinflammation, J. Thromb. Haemostasis 20 (7) (2022) 1535–1549.
[15] B. Huang, M. Bates, X. Zhuang, Super-resolution fluorescence microscopy, Annu. Rev. Biochem. 78 (2009) 993–1016.
[16] A.C. Swanepoel, E. Pretorius, Ultrastructural analysis of platelets during three phases of pregnancy: a qualitative and quantitative investigation, Hematology 20 (1) (2015) 39–47.
[17] J. Kamykowski, et al., Quantitative immunofluorescence mapping reveals little functional coclustering of proteins within platelet α-granules, Blood 118 (5) (2011) 1370–1373.
[18] S. Yadav, B. Storrie, The cellular basis of platelet secretion: emerging structure/function relationships, Platelets 28 (2) (2017) 108–118.
[19] M.J. Rust, M. Bates, X. Zhuang, Sub-diffraction-limit imaging by stochastic optical reconstruction microscopy (STORM), Nat. Methods 3 (10) (2006) 793–795.
[20] E. Betzig, et al., Imaging intracellular fluorescent proteins at nanometer resolution, Science 313 (5793) (2006) 1642–1645.
[21] S.T. Hess, T.P. Girirajan, M.D. Mason, Ultra-high resolution imaging by fluorescence photoactivation localization microscopy, Biophys. J. 91 (11) (2006) 4258–4272.
[22] J.W. Lichtman, J.A. Conchello, Fluorescence microscopy, Nat. Methods 2 (12) (2005) 910–919.
[23] A.O. Khan, J.A. Pike, Super-resolution imaging and quantification of megakaryocytes and platelets, Platelets 31 (5) (2020) 559–569.
[24] Y. Hirano, A. Matsuda, Y. Hiraoka, Recent advancements in structured-illumination microscopy toward live-cell imaging, Microscopy (Lond.) 64 (4) (2015) 237–249.
[25] Z. Yang, et al., Super-resolution microscopy for biological imaging, Adv. Exp. Med. Biol. 3233 (2021) 23–43.
[26] S. Liu, P. Hoess, J. Ries, Super-resolution microscopy for structural cell biology, Annu. Rev. Biophys. 51 (2022) 301–326.
[27] A. Li, et al., Comparison of ultrastructural and nanomechanical signature of platelets from acute myocardial infarction and platelet activation, Biochem. Biophys. Res. Commun. 486 (2) (2017) 245–251.
[28] R. Wang, et al., Electron cryotomography reveals ultrastructure alterations in platelets from patients with ovarian cancer, Proc. Natl. Acad. Sci. U. S. A. 112 (46) (2015) 14266–14271.
[29] D. Westmoreland, et al., Super-resolution microscopy as a potential approach to diagnosis of platelet granule disorders, J. Thromb. Haemostasis 14 (4) (2016) 839–849.
[30] K. Kang, et al., Dishevelled phase separation promotes Wnt signalosome assembly and destruction complex disassembly, J. Cell Biol. 221 (12) (2022).
[31] A. Butola, et al., Scalable-resolution structured illumination microscopy, Opt Express 30 (24) (2022) 43752–43767.
[32] M.G. Gustafsson, Surpassing the lateral resolution limit by a factor of two using structured illumination microscopy, J. Microsc. 198 (Pt 2) (2000) 82–87.
[33] Y. Wu, H. Shroff, Faster, sharper, and deeper: structured illumination microscopy for biological imaging, Nat. Methods 15 (12) (2018) 1011–1019.
[34] S. Wäldchen, et al., Light-induced cell damage in live-cell super-resolution microscopy, Sci. Rep. 5 (2015), 15348.
[35] L. Schermelleh, et al., Super-resolution microscopy demystified, Nat. Cell Biol. 21 (1) (2019) 72–84.
[36] J. Demmerle, et al., Strategic and practical guidelines for successful structured illumination microscopy, Nat. Protoc. 12 (5) (2017) 988–1010.
[37] M. Swinkels, et al., Quantitative 3D microscopy highlights altered von Willebrand factor α-granule storage in patients with von Willebrand disease with distinct pathogenic mechanisms, Res. Pract. Thromb. Haemost. 5 (6) (2021), e12595.
[38] J.M. Pullman, et al., Visualization of podocyte substructure with structured illumination microscopy (SIM): a new approach to nephrotic disease, Biomed. Opt Express 7 (2) (2016) 302–311.
[39] J. Liu, et al., Nondestructive diagnosis of kidney cancer on 18-gauge core needle renal biopsy using dual-color fluorescence structured illumination microscopy, Urology 98 (2016) 195–199.
[40] W. Lu, et al., Morphology of platelet Golgi apparatus and their significance after acute cerebral infarction, Neural. Regen. Res. 8 (23) (2013) 2134–2143.
[41] R. Joseph, et al., Platelet ultrastructure and secretion in acute ischemic stroke, Stroke 20 (10) (1989) 1316–1319.
[42] S.L. Allford, S.J. Machin, Current understanding of the pathophysiology of thrombotic thrombocytopenic purpura, J. Clin. Pathol. 53 (7) (2000) 497–501.
[43] J. Chen, D.W. Chung, Inflammation, von Willebrand factor, and ADAMTS13, Blood 132 (2) (2018) 141–147.
[44] H.R. Gralnick, et al., Platelet von Willebrand factor, Mayo Clin. Proc. 66 (6) (1991) 634–640.
[45] M.C. van Schie, et al., von Willebrand factor propeptide and the occurrence of a first ischemic stroke, J. Thromb. Haemostasis 8 (6) (2010) 1424–1426.
[46] M. Kannan, F. Ahmad, R. Saxena, Platelet activation markers in evaluation of thrombotic risk factors in various clinical settings, Blood Rev. 37 (2019), 100583.
[47] S.L. Haberichter, von Willebrand factor propeptide: biology and clinical utility, Blood 126 (15) (2015) 1753–1761.
[48] U.M. Vischer, et al., von Willebrand factor (vWf) as a plasma marker of endothelial activation in diabetes: improved reliability with parallel determination of the vWf propeptide (vWf:AgII), Thromb. Haemostasis 80 (6) (1998) 1002–1007.
[49] E.J. Bowie, et al., Transplantation of normal bone marrow into a pig with severe von Willebrand's disease, J. Clin. Invest. 78 (1) (1986) 26–30.
[50] R. Schuppner, et al., ADAMTS-13 activity predicts outcome in acute ischaemic stroke patients undergoing endovascular treatment, Thromb. Haemostasis 118 (4) (2018) 758–767.
[51] M. Scully, et al., Regional UK TTP registry: correlation with laboratory ADAMTS 13 analysis and clinical features, Br. J. Haematol. 142 (5) (2008) 819–826.
[52] P.J. Lenting, C.V. Denis, Platelet von Willebrand factor: sweet resistance, Blood 122 (25) (2013) 4006–4007.
[53] K. Yamamoto, et al., Tissue distribution and regulation of murine von Willebrand factor gene expression in vivo, Blood 92 (8) (1998) 2791–2801.
[54] P. Gong, et al., The association of neutrophil to lymphocyte ratio, platelet to lymphocyte ratio, and lymphocyte to monocyte ratio with post-thrombolysis early neurological outcomes in patients with acute ischemic stroke, J. Neuroinflammation 18 (1) (2021) 51.
[55] R. Bi, et al., The role of leukocytes in acute ischemic stroke-related thrombosis: a notable but neglected topic, Cell. Mol. Life Sci. 78 (17–18) (2021) 6251–6264.
[56] X. Blanchet, et al., Inflammatory role and prognostic value of platelet chemokines in acute coronary syndrome, Thromb. Haemostasis 112 (6) (2014) 1277–1287.
[57] Y. Zhang, et al., Clinical significance of PAC-1, CD62P, and platelet-leukocyte aggregates in acute ischemic stroke, Bull. Exp. Biol. Med. 172 (5) (2022) 543–548.
[58] S.F. Mause, et al., Platelet microparticles: a transcellular delivery system for RANTES promoting monocyte recruitment on endothelium, Arterioscler. Thromb. Vasc. Biol. 25 (7) (2005) 1512–1518.
[59] C.A. Gleissner, Macrophage phenotype modulation by CXCL4 in atherosclerosis, Front. Physiol. 3 (2012) 1.
[60] C.A. Gleissner, et al., CXCL4 downregulates the atheroprotective hemoglobin receptor CD163 in human macrophages, Circ. Res. 106 (1) (2010) 203–211.

[61] J. Cui, et al., Thrombo-inflammation and immunological response in ischemic stroke: focusing on platelet-tregs interaction, Front. Cell. Neurosci. 16 (2022), 955385.
[62] Y. Fan, et al., MKEY, a peptide inhibitor of CXCL4-CCL5 heterodimer formation, protects against stroke in mice, J. Am. Heart Assoc. 5 (9) (2016).
[63] C.D. Garlichs, et al., Upregulation of CD40-CD40 ligand (CD154) in patients with acute cerebral ischemia, Stroke 34 (6) (2003) 1412–1418.
[64] G.P. Mulley, et al., ADP-induced platelet release reaction in acute stroke, Thromb. Haemostasis 50 (2) (1983) 524–526.
[65] D.O. Kleindorfer, et al., Guideline for the prevention of stroke in patients with stroke and transient ischemic attack: a guideline from the American heart association/American stroke association, Stroke 52 (7) (2021) e364–e467.
[66] Y. Gao, et al., The role of P2Y(12) receptor in ischemic stroke of atherosclerotic origin, Cell. Mol. Life Sci. 76 (2) (2019) 341–354.
[67] J.M. Cosemans, et al., Multiple ways to switch platelet integrins on and off, J. Thromb. Haemostasis 6 (8) (2008) 1253–1261.
[68] A.C.A. Heinzmann, et al., Combined antiplatelet therapy reduces the proinflammatory properties of activated platelets, TH Open 5 (4) (2021) e533–e542.
[69] D. Li, et al., Roles of purinergic receptor P2Y, G protein-coupled 12 in the development of atherosclerosis in apolipoprotein E-deficient mice, Arterioscler. Thromb. Vasc. Biol. 32 (8) (2012) e81–e89.
[70] H.Y. Huang, et al., Effectiveness and safety of clopidogrel vs aspirin in elderly patients with ischemic stroke, Mayo Clin. Proc. 97 (8) (2022) 1483–1492.
[71] M. Paciaroni, et al., Benefits and risks of clopidogrel vs. Aspirin monotherapy after recent ischemic stroke: a systematic review and meta-analysis, Cardiovasc. Ther. 2019 (2019), 1607181.
[72] X. Niu, et al., P2Y(12) promotes migration of vascular smooth muscle cells through cofilin dephosphorylation during atherogenesis, Arterioscler. Thromb. Vasc. Biol. 37 (3) (2017) 515–524.
[73] A. Sugidachi, et al., The active metabolite of prasugrel, R-138727, improves cerebral blood flow and reduces cerebral infarction and neurologic deficits in a non-human primate model of acute ischaemic stroke, Eur. J. Pharmacol. 788 (2016) 132–139.
[74] C. Heim, et al., Clopidogrel significantly lowers the development of atherosclerosis in ApoE-deficient mice in vivo, Heart Ves. 31 (5) (2016) 783–794.